Molecular recognition of structurally disordered Pro/Ala-rich sequences (PAS) by antibodies involves an Ala residue at the hot spot of the epitope

J. Schilz [1], U. Binder [2], L. Friedrich [2], M. Gebauer [2], C. Lutz [1], M. Schlapschy [1], A. Schiefner [1] and A. Skerra [1,2]*

*1 - **Lehrstuhl für Biologische Chemie,** Technische Universität München, Emil-Erlenmeyer-Forum 5, 85354 Freising, Germany*
*2 - **XL-protein GmbH,** Lise-Meitner-Strasse 30, 85354 Freising, Germany*

***Correspondence to A. Skerra:** skerra@tum.de (A. Skerra)*
https://doi.org/10.1016/j.jmb.2021.167113
Edited by S. Koide

Abstract

Pro/Ala-rich sequences (PAS) are polypeptides that were developed as a biological alternative to polyethylene glycol (PEG) to generate biopharmaceuticals with extended plasma half-life. Like PEG, PAS polypeptides are conformationally disordered and show high solubility in water. Devoid of any charged or prominent hydrophobic side chains, these biosynthetic polymers represent an extreme case of intrinsically disordered proteins. Despite lack of immunogenicity of PAS tags in numerous animal studies we now succeeded in generating monoclonal antibodies (MAbs) against three different PAS versions. To this end, mice were immunized with a PAS#1, P/A#1 or APSA 40mer peptide conjugated to keyhole limpet hemocyanin as highly immunogenic carrier protein. In each case, one MAb with high binding activity and specificity towards a particular PAS motif was obtained. The apparent affinity was strongly dependent on the avidity effect and most pronounced for the bivalent MAb when interacting with a long PAS repeat. X-ray structural analysis of four representative anti-PAS Fab fragments in complex with their cognate PAS epitope peptides revealed interactions dominated by hydrogen bond networks involving the peptide backbone as well as multiple Van der Waals contacts arising from intimate shape complementarity. Surprisingly, Ala, the L-amino acid with the smallest side chain, emerged as a crucial feature for epitope recognition, contributing specific contacts at the center of the paratope in several anti-PAS complexes. Apart from these insights into how antibodies can recognize feature-less peptides without secondary structure, the MAbs characterized in this study offer valuable reagents for the preclinical and clinical development of PASylated biologics.

Introduction

Intrinsically disordered proteins (IDPs) or protein domains are common in nature and play important roles in mediating signal transduction and protein trafficking, where the conformational flexibility of IDPs allows interactions with multiple targets at moderate affinity.[1–3] IDPs are also abundant in many pathogens and, thus, represent potential targets to combat infectious diseases.[4] In contrast to the specific interactions with structured proteins, the biophysical properties of disordered peptides or polypeptide segments often pose a challenge for the immune system in the generation of cognate antibodies, a feature that even seems to be exploited by pathogens to evade an immune response.[5,6]

Common antigens of the immune system are mostly proteins or peptides whose surface epitopes act as points of interaction for the

specific recognition by antibodies. Epitopes are generally divided into two categories, (i) linear epitopes that are defined by their primary structure and (ii) conformational or discontinuous epitopes, where the key amino acids are separated in the amino acid sequence but brought into close proximity by the three-dimensional fold.[7] It has long been assumed that potent epitopes are predominantly discontinuous;[7] in fact, more recent analyses suggest that such conformational epitopes constitute about 90% of all B-cell epitopes present in native proteins.[8]

While intermolecular interactions involving disordered proteins have been analysed in detail,[9–11] only a few studies have addressed the structural aspects of complex formation between flexible protein antigens and rigid binding partners such as antibodies.[12,13] Structural analyses of a large dataset of protein antigens have shown that residues in unstructured linear epitopes are more likely involved in hydrogen bonds and salt bridges than those in conformational epitopes. Furthermore, IDPs present smaller epitopes than folded antigens whereas they appear to have more extensive contacts per residue and a higher shape complementarity with their cognate antibody.[12] In general, the interfaces formed by unstructured peptides and their antibodies are dominated by hydrogen bonds, often involving the peptide backbone, and they tend to bind in a more planar fashion if compared to folded proteins; moreover, the peptide interfaces are enriched in large hydrophobic side chains, such as Phe, Leu, Trp, Tyr and Ile, which serve as hot spot for binding.[14]

In the last decade, designed structurally disordered polypeptides have gained attention in the field of pharmaceutical biotechnology, where they are used to extend the *in vivo* half-life of protein fusion partners or drug conjugates as a biodegradable alternative to poly-ethylene glycol (PEG).[15,16] In particular, long polypeptides comprising the small, uncharged L-amino acids Pro, Ala and/or Ser (PAS) show high solubility and macromolecular properties closely similar to the hydrophilic and structurally disordered PEG.[17] Indeed, PASylation of pharmacologically active proteins or peptides dramatically expands their hydrodynamic volume and prolongs the *in vivo* half-life by effectively retarding renal filtration.[18]

PAS polypeptides are devoid both of charged and of bulky hydrophobic side chains, which normally play a role for molecular recognition in the immune response.[19] On the other hand, their strong hydrophilicity is explained by the exposure of the polar peptide groups to the aqueous solvent in the absence of secondary structure.[17] In addition, their random coil behaviour under physiological conditions poses a huge entropic cost for the disorder-to-order transition upon complex formation with antibodies. In fact, in numerous *in vivo* imaging studies with PASylated antibody fragments as well as in preclinical animal experiments involving repeated administration of PASylated protein drugs at high doses, neither unspecific binding to any receptors nor a PAS-specific immune response was evident.[20–24]

To investigate potential mechanisms how the immune system may recognize structurally disordered PAS (poly)peptides, which provide an extreme model of natural IDPs with a virtually feature-less amino acid sequence, we set out to elicit antibodies against different PAS peptides and elucidate the resulting antigen-antibody complexes at the structural level.

Results

We have raised mouse monoclonal antibodies (MAbs) against three different PAS polypeptides: PAS#1, P/A#1 and APSA (Figure 1). To this end, five animals per antigen were immunized with the corresponding synthetic N-terminally protected 40mer peptide, which had been chemically coupled via the unique C-terminal carboxylate group to mariculture keyhole limpet hemocyanin (KLH) as a highly immunogenic T-cell dependent carrier antigen.[25] In the case of PAS#1 and P/A#1 the 40mer covered exactly two copies of the designed 20mer sequence repeat as published before,[16,17] whereas the "APSA" peptide comprised 10 copies of a short 4-residue motif and may be considered as a simplified kind of Pro/Ala-rich sequence. The PAS#1 and P/A#1 peptide immunogens were designed to include at least one copy of the junction between two adjacent 20mer sequence repeats, which can also potentially contribute an epitope in longer recombinant PAS polypeptides.

After four to six rounds of intensive immunization as well as a final boost, each with 25–50 μg antigen, spleen cells were isolated from the mouse with the highest signal in a serum ELISA for each antigen and fused with Sp2/0 myeloma cells to generate hybridomas.[26] Prescreening of 960 hybridoma culture supernatants obtained for each of these mice in an enzyme-linked immunosorbent assay (ELISA) against a suitable PAS fusion protein revealed around 10% positive clones. Antibodies from the top 40 hybridoma clones were subsequently characterized in detail by ELISA, using recombinant fusion proteins comprising the corresponding PAS polypeptide (200–600 residues in conjunction with a Fab fragment, IL-1Ra or GMCSF; for details, see Materials and Methods), with the goal of (i) screening for sequence-specific and context-independent recognition of PAS-sequences and (ii) potentially identifying antibodies that show cross-reactivity between different PAS sequences. To this end, IgG capture ELISAs with hybridoma culture supernatants were performed, applying the PAS fusion protein in a concentration-dependent manner in order to determine the dissociation con-

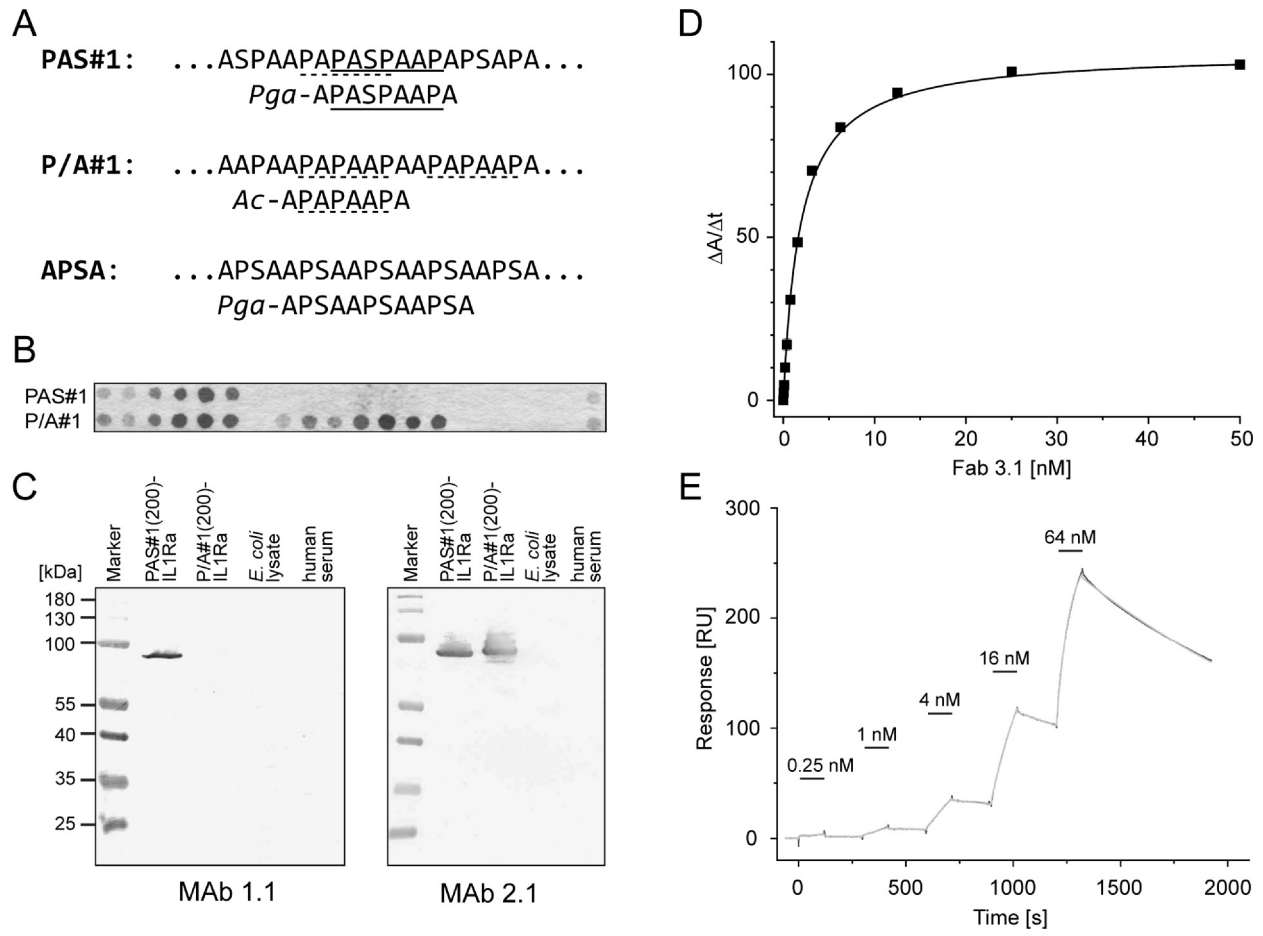

Figure 1. Functional properties of anti-PAS MAbs. (A) Amino acid sequence of the basic repetitive 20mer units of PAS#1 and P/A#1 polypeptides as well as a 20mer stretch comprising 5 copies of the APSA sequence motif. Epitope sequences evident from the SPOT assay for the anti-PAS#1 and anti-P/A#1 (broken line) MAbs are underlined. The corresponding synthetic peptides with blocked N-termini that were used for co-crystallization experiments are aligned underneath (*Pga*: pyroglutamyl; *Ac*: acetyl). (B) Exemplary SPOT assay for the Fab 2.1. Consecutive 12-mer peptides from the PAS#1 (upper row) and P/A#1 (lower row) repeat units, each shifted by one residue, where synthesized C-terminally anchored on a hydrophilic membrane. The results of all SPOT assays are shown in Supplementary Figure S5. (C) Detection of PASylated fusion proteins on western blots with the hybridoma culture supernatants of clones 1.1 and 2.1. (D) Direct ELISA with the Fab 3.1 and APSA(200)-IL1Ra adsorbed to the microtiter plate, followed by a secondary antibody. (E) SPR sensorgram for Fab 3.1 as analyte with biotinylated TrxA-APSA(200) as immobilized ligand. Injection phases are labeled with black bars, together with the corresponding concentration of injected analyte (black, raw signal trace; gray, curve fit).

stants (K_D). Hybridoma culture supernatants harbouring promising MAb candidates were further characterized with regard to antigen affinity and binding kinetics by real-time surface plasmon resonance (SPR) spectroscopy. Exemplary ELISA and SPR results are shown in the Supplementary Information (Figures S1–S3).

Based on the K_D values resulting from the ELISA and SPR measurements (also considering the absorption amplitudes in the concentration-dependent ELISAs), 3–8 non-redundant clones with distinct properties were selected from the immunization with PAS#1(40)-KLH, P/A#1(40)-KLH and APSA(40)-KLH, respectively. Of these, the two most promising hybridoma clones for each PAS antigen were selected for further analysis using both their affinities to the target sequences as well as signs of cross-reactivity with other PAS sequences as criteria: MAbs 1.1 and 1.2 for PAS#1, MAbs 2.1 and 2.2 for P/A#1, MAbs 3.1 and 3.2 for APSA. To verify applicability of these MAbs for the detection of PASylated fusion proteins, the corresponding hybridoma culture supernatants were finally tested in western blotting experiments wherein the specific detection of PASylated fusion proteins was confirmed (Figures 1 and S4). Notably, no cross-reactivity with the non-PASylated fusion partner, human serum proteins or an *E. coli* whole cell protein extract was observed.

These MAbs were further tested for linear epitope recognition using the Synthetic Peptides On Transfer membranes (SPOT) technique.[27] This assay revealed the same predominant peptide motif "PASPAAP" for the anti-PAS#1 MAbs 1.1 and 1.2 whereas the peptide motifs "PAPAAP" and also "PAPASP" were recognized by both anti-P/A#1 MAbs 2.1 and 2.2 (Figures 1(A) and S5). Due to the simpler and highly repetitive nature of the APSA target sequence, a SPOT substitution analysis was performed for the two most promising MAbs selected against this antigen. Therefore, a 10mer peptide comprising the sequence AAPSAAPSAA was systematically substituted at positions 3 to 8 by all 20 proteinogenic amino acids. This analysis revealed the importance of the linear "PSAA(PS)" epitope for recognition by both anti-APSA MAbs 3.1 and 3.2 (Figures 1(A) and S5). As result of the SPOT epitope analysis, MAbs generated by immunization with PAS#1(40)-KLH only recognize the PAS#1 polypeptide sequence (MAb 1.1 and MAb 1.2), while both MAbs from the P/A#1(40)-KLH immunization (MAb 2.1 and MAb 2.2) show cross-reactivity with PAS#1 in addition to the P/A#1 epitope. Tentatively, a generalized sequence motif recognized by all MAbs, including those raised against the APSA sequence, emerged as "(P/S)A(A/S)P".

In the next step, the V_H and V_L sequences of the six MAbs were determined from each hybridoma mRNA (Figure 2). All sequences showed the typical pattern of mouse immunoglobulin (Ig) V-regions, and the complementarity-determining regions (CDRs) were easily identifiable. Notable features were (i) a very long CDR-L1 in all six MAbs, with 4–6 residues inserted at the middle according to the Kabat numbering scheme,[28] (ii) the very short CDR-H3 sequences of MAbs 3.1 and 3.2, with only three and five residues, respectively, as well as (iii) an unpaired Cys residue in the framework region (FR) 2 of MAb 3.2. For subsequent production of the recombinant Fab fragments in *E. coli*, suitable coding regions were derived by reverse-transcription of mRNA and cDNA amplification via polymerase chain reaction (PCR), or obtained as synthetic DNA fragments, and inserted into a bacterial expression vector which encoded already the first human IgG1 heavy chain and κ light chain constant regions.[29,30] The chimeric Fab fragments were produced in a functional state by periplasmic secretion in *E. coli* both at the shake flask and at the bench top fermenter scale and purified to homogeneity.

The recombinant Fabs were investigated in quantitative ELISAs and real-time SPR measurements in comparison with the corresponding MAbs from the hybridoma culture supernatants in order to precisely determine their K_D values towards the different PAS polypeptides (Table 1). These measurements essentially confirmed the findings from the preliminary hybridoma screening study described above. In each case, just one antibody with outstanding affinity was identified for the different PAS antigens as judged from a K_D value in the lower nM range measured in the ELISA for the monovalent Fab: 23 nM *versus* PAS#1 (Fab 1.1), 2 nM *versus* P/A#1 (Fab 2.1) and 2 nM *versus* APSA (Fab 3.1). Of note, compared with the results for the hybridoma culture supernatants, the affinities measured for the Fabs in the ELISA were typically by 1–2 orders weaker. This was most likely due to the avidity effect that arises when the bivalent MAb interacts with a long PAS polypeptide which harbours multiple copies of the epitope – such as, for example, 30 copies of the repetitive PAS#1 amino acid stretch in a 600-residue PAS polypeptide. Remaining differences between the values measured by SPR and ELISA can be explained by the variations in the experimental setup. Interestingly, both anti-P/A#1 Fabs showed cross-reactivity with the PAS#1 sequence as noted for their respective MAbs in the SPOT assay described above, whereas the anti-APSA Fab 3.2 and also the MAb 3.2 showed weaker cross-reactivity with both PAS#1 and P/A#1 polypeptides (Table 1).

Finally, the structural mechanism of antigen recognition was analyzed for several of these anti-PAS Fabs via X-ray crystallography. To this end, co-crystallization experiments were performed with the cognate synthetic peptides, whose sequences were either based on the findings of the SPOT epitope search as described above or, in case of the simple APSA motif, comprised a 12-residue stretch with three APSA repeats. To avoid charges at the N-termini, which would be absent in longer PAS (poly)peptides, these were blocked with pyroglutamic acid (Pga) or by acetylation. Diffraction quality crystals were directly obtained for the Fab•peptide complexes 1.1, 2.2 and 3.1 (Table S1) whereas in the case of the Fab 1.2 a recently published strategy employing an anti-human kappa light chain V_HH domain to facilitate (co)-crystallization[31] was successfully applied.

Analysis of these crystal structures (Figure 3) showed that the different PAS peptides are bound to all four Fabs in a more or less relaxed conformation, covering a wide area of the antigen-binding site with at least four of the six CDRs involved. Due to the lack of pronounced hydrophobic as well as polar side chains – except for one Ser residue in the PAS#1 epitope peptide and three Ser residues in the $(APSA)_3$ peptide – the interactions are predominantly mediated through hydrogen bonds with the peptide main-chain groups (Table S2) as well as Van der Waals contacts (Table S3). As expected, salt bridges are completely absent. In the structures of the Fabs 1.2 and 3.1, some of these hydrogen bond interactions are mediated by water molecules. Surface representations illustrating electrostatic and hydrophobic properties reveal hydrophobic

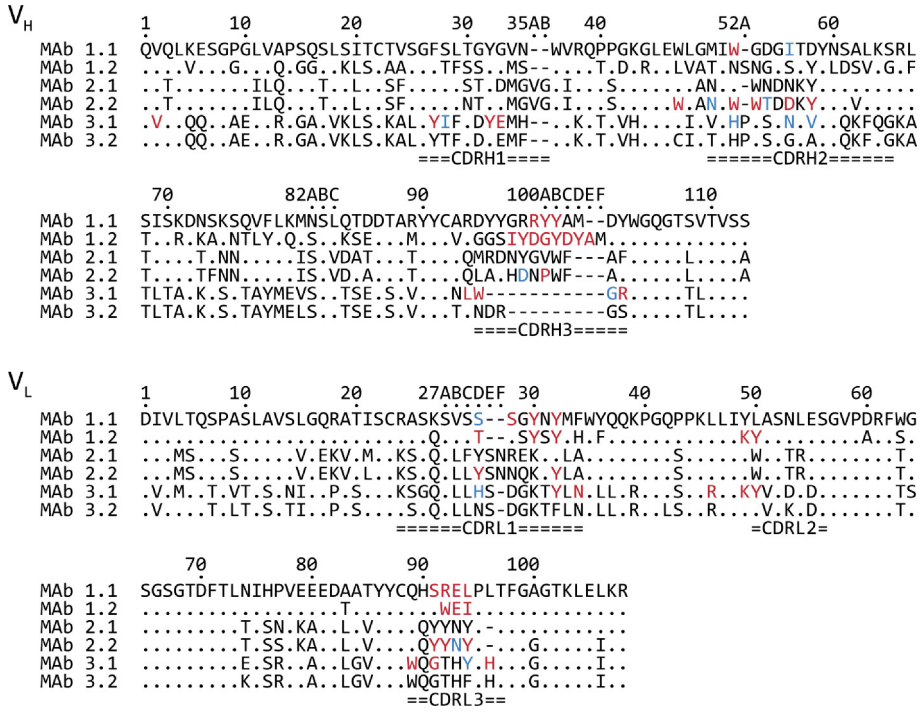

Figure 2. Amino acid sequence alignment for the V_H and V_L domains of the Avi-PA(S) MAbs described in this study (prior to the introduction of flanking restriction sites for subcloning) using *ANTIC*ALIgN software.[74] CDRs are labelled, and conserved amino acid positions are shown as "." whereas gaps are indicated by "-". For better comparison, sequences in this alignment are numbered according to Kabat[28] whereas in the text and the other Figures, like in the PDB coordinate sets, sequential numbering has been used. Contact residues in the paratopes are coloured blue or, if germline-encoded, red.

Table 1 Affinities of the MAbs and corresponding Fabs towards their cognate PAS (poly)peptides measured by ELISA and SPR.

			Antigen					
			PAS#1		P/A#1		APSA	
		Avi-PA(S) MAb	1.1	1.2	2.1	2.2	3.1	3.2
Format	Assay	Target						
MAb	SPR	PAS#1(200)-IL1Ra	1.0 ± 0.1 nM	44 ± 1 nM	1.7 ± 0.1 nM	22 ± 1 nM	n.q.	80 ± 3 nM
MAb	ELISA	hu4D5-PAS#1(200)	37 ± 10 pM	162 ± 11 pM	113 ± 11 pM	n.q.	n.q.	294 ± 92 pM
Fab	SPR	PAS#1(200)-IL1Ra	8.8 ± 0.4 μM	3.7 ± 0.2 μM	4.4 ± 0.4 μM	n.d.	n.d.	n.q.
Fab	ELISA	PAS#1(600)-Leptin	23 ± 5 nM	123 ± 20 nM	2.2 ± 0.1 nM	n.q.	n.q.	311 ± 16 nM
MAb	SPR	P/A#1(200)-IL1Ra	n.q.	n.q.	429 ± 23 pM	1.1 ± 0.1 nM	n.q.	20 ± 1 nM
MAb	ELISA	hu4D5-P/A#1(200)	n.q.	n.q.	170 ± 31 pM	69 ± 9 pM	n.q.	400 ± 100 pM
Fab	SPR	P/A#1(200)-IL1Ra	n.d.	n.d.	648 ± 29 nM	7.0 ± 0.2 μM	n.d.	446 ± 34 nM
Fab	ELISA	P/A#1(600)	n.q.	n.q.	2.0 ± 0.2 nM	8 ± 1 nM	n.q.	48 ± 4 nM
MAb	SPR	APSA(200)-IL1Ra	n.q.	n.q.	n.q.	n.q.	19 ± 1 pM	108 ± 2 pM
MAb	ELISA	APSA(200)-IL1Ra	n.q.	n.q.	n.q.	n.q.	118 ± 2 pM	251 ± 5 pM
Fab	SPR	APSA(200)-TrxA	n.d.	n.d.	n.d.	n.d.	2.5 ± 0.1 nM	137 ± 8 nM
Fab	ELISA	APSA(200)-IL1Ra	n.d.	n.d.	n.d.	n.d.	1.9 ± 0. 1 nM	1.6 ± 0.1 nM

n.q.: not quantifiable; n.d.: not determined.

areas with slightly negative potential for all paratopes, except for one cavity with slightly positive potential in the structure of the Fab 3.1 (Figure S6). Interestingly, in each case at least one Ala residue of the PAS epitope peptide is involved in relevant interactions with the anti-PAS Fab.

In the crystal structure of the Fab 1.1 in complex with the PAS#1 epitope peptide, the peptide ligand extends across a large area of the

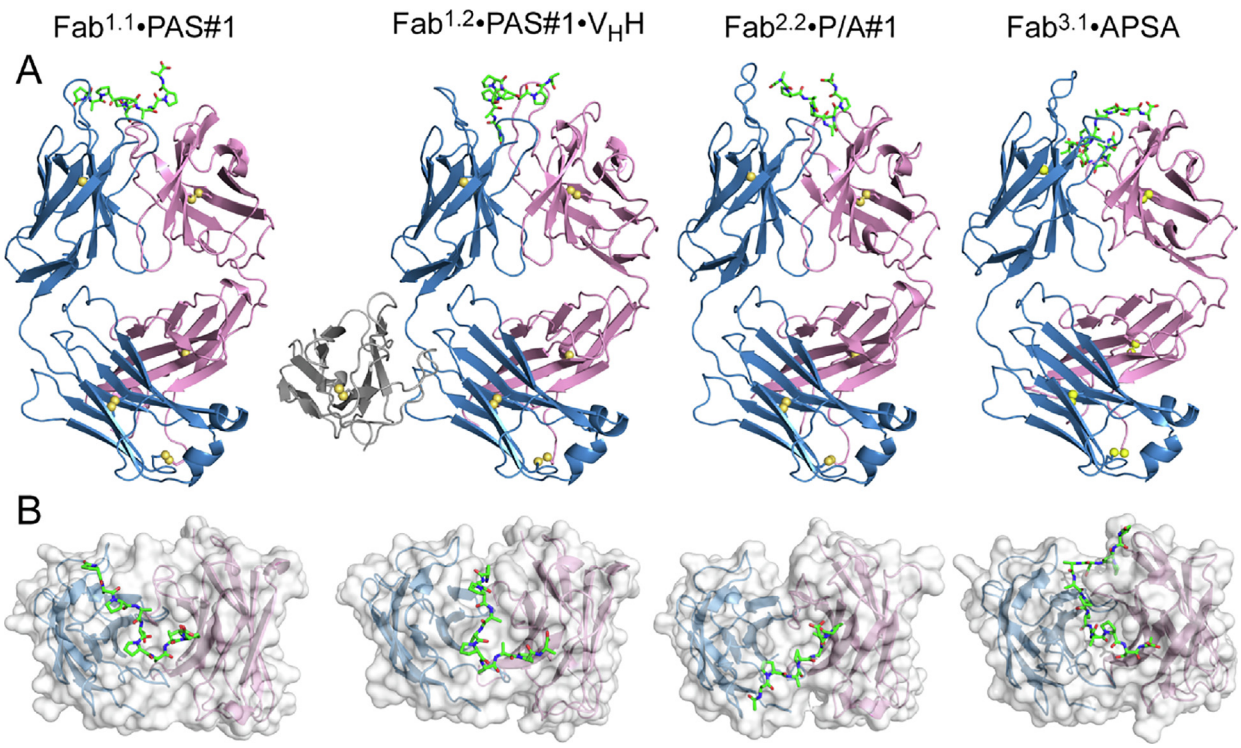

Figure 3. Crystal structures of the Fabs 1.1, 1.2, 2.2 and 3.1 in complex with PAS peptides. (A) Cartoon representation of the full Fab (light chain: blue; heavy chain: pink), each with its bound epitope peptide (green). Disulphide bonds are depicted as ball-and-sticks with sulphur atoms coloured yellow. The anti-human κ light chain V_HH domain that served as crystallization helper for the Fab 1.2 is shown in grey. (B) Top view on the antigen-binding sites, colouring as in (A), and Fv regions displayed with translucent surfaces.

paratope, engaging 579 Å^2 of its accessible surface area (ASA). The peptide forms a turn with its residues Ser^{P5}–Ala^{P8} at the center of the paratope which, together with the N-terminal residues Ala^{P2}–Ala^{P4}, is responsible for the majority of contacts. In contrast, the three C-terminal amino acids point away from the antigen-binding site into the solvent and are only sparsely involved in the complex. The peptide backbone forms three hydrogen bonds with the Fab residues Tyr^{L36} (CDR-L1), which is bound to Pro^{P3}, and Arg^{H103} (CDR-H3), which is bound to both Ser^{P5} and Pro^{P9} (Table S2). In addition, there is a hydrogen bond from the hydroxyl group of the only polar side chain in the epitope peptide, Ser^{P5}, to the carbonyl oxygen of Ser^{L95} in CDR-L3. Apart from that, the paratope exhibits distinct hydrophobic surface patches to accommodate the non-polar atomic groups of the peptide. For example, Tyr^{L34} has its aromatic ring positioned next to Ala^{P2} and, together with Leu^{L54}, provides a suitable hydrophobic environment for the methyl side chain. Another Ala residue of the PAS peptide, Ala^{P7}, plays a central role for the complex formation: its small side chain points right into a hole with slightly negative potential in the antigen-binding site which is shaped by the residues Ser^{L95}, Arg^{L96}, Glu^{L97}, Leu^{L98} and also Leu^{L100} in CDR-L3 and Tyr^{H105} in CDR-H3 (Figure 4(A) and Table S3). This hole and the methyl side chain show perfect shape complementarity, allowing dense interaction between the Fab and the PAS#1 epitope peptide (Table S4).

In the structure of the Fab 1.2 in complex with the same peptide, the PAS#1 epitope is bound in a groove formed by the light chain CDRs on one side and CDR-H3 on the other (Figure 4(B)), thereby involving a peptide ASA of 652 Å^2. Again, its N-terminal residues are well accommodated and provide the majority of interactions with the Fab (Table S3). In particular, Ala^{P2} is tightly nestled within the groove, with >90% of its ASA buried (Table S4) by the side chains of Tyr^{L34}, Tyr^{L36} and Tyr^{L54} from the antibody light chain, which form a hydrophobic cage around this residue (Figure 4(D)). Residues in CDR-H3 mediate five of in total seven hydrogen bonds to the peptide main chain. The three N-terminal residues of the peptide are engaged in a hydrogen bond network with the main chain of CDR-H3 that resembles a short antiparallel β-sheet (Figure 4 (F)). Similar to the Fab 1.1 in complex with the PAS#1 peptide, the Fab 1.2 targets the only polar side chain, Ser^{P5}, this time by forming a hydrogen

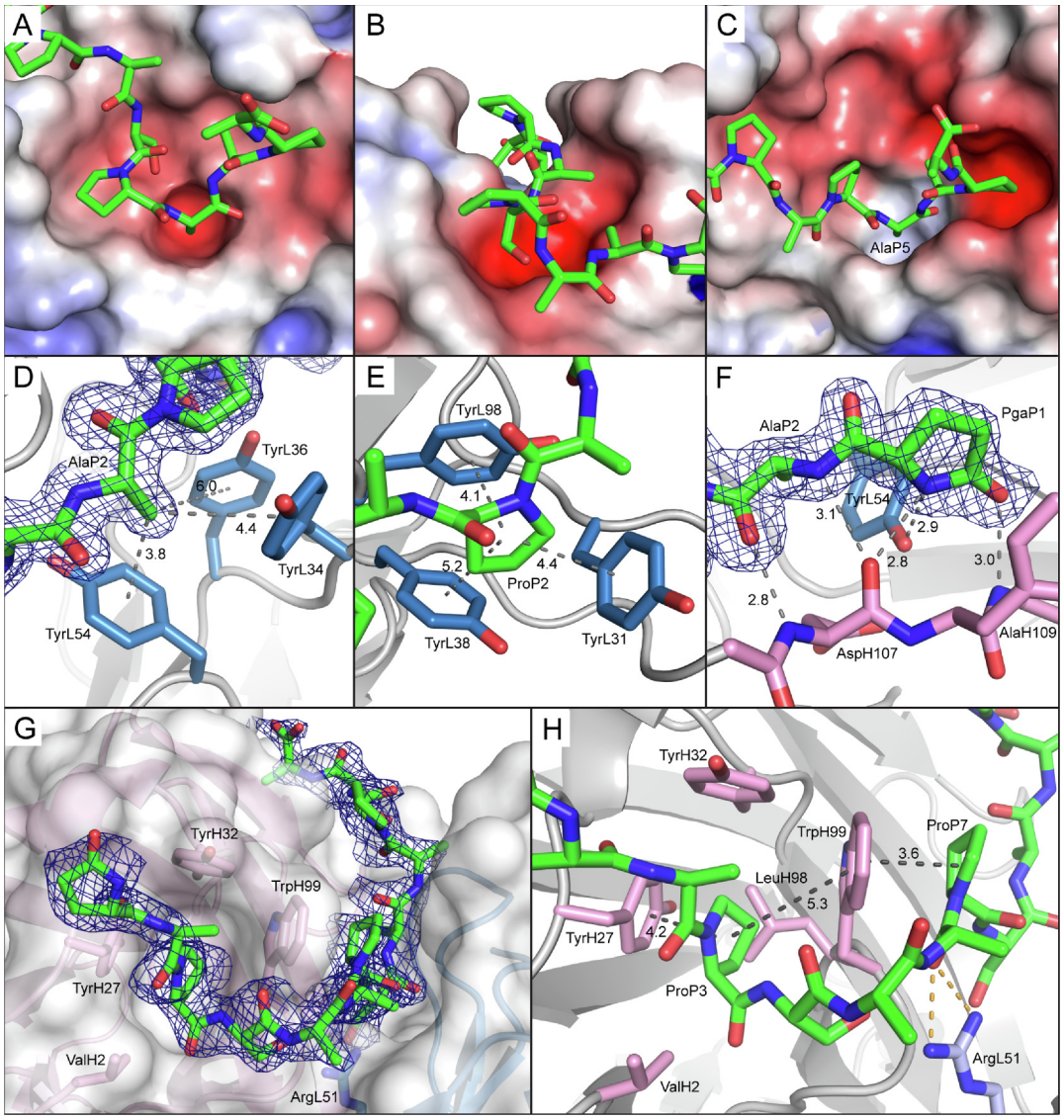

Figure 4. Structural details of PAS peptide recognition. (A-C) Electrostatic surface representations of anti-PAS MAb binding sites with negative potential coloured red (-5 k_BT/e) and positive potential coloured blue (5 k_BT/e). (A) Paratope of Fab 1.1 with Ala^{P7} pointing right into a central hole. (B) Paratope of Fab 1.2 with the N-terminal residues of the PAS epitope peptide nestled in the groove formed by the light chain CDRs and CDR-H3. (C) Binding pocket of Fab 2.2 burying Ala^{P5} at the centre of the epitope. (D-F) Close-up view on interactions between Fabs and the bound PAS peptides. Relevant distances are indicated as grey dashed lines with values given in Å. Cages of Tyr side chains are formed around part of the PAS peptides by the Fab 1.2 (D) and Fab 2.2 (E). (F) Backbone hydrogen bond network between the Fab 1.2 and the bound PAS#1 epitope peptide, including the N-terminal Pga group. (G) Accommodation of the $(APSA)_3$-peptide within the paratope of Fab 3.1 and (H) stacking interactions between Tyr^{H27}, Pro^{P3}, Trp^{H99} and Pro^{P7} (black dashed lines) as well as the bifurcated hydrogen bonding by Arg^{L51} (orange dashed lines) in Fab 3.1. The $2F_O$-F_C electron density map is displayed at a contour level of 1σ (D, F and G).

bond with the main chain carbonyl oxygen of Trp^{L96} (CDR-L3). Notably, the N-terminal Pga group of the peptide contributes to complex formation with three hydrogen bonds to Tyr^{L54} (CDR-L2), Asp^{H107} and Ala^{H109} (the latter residues in CDR-H3). These hydrogen bonds would not be possible in a complex with a longer PAS#1 (poly)peptide where the position of the Pga residue would be occupied by Pro. While the Pro residue itself could perfectly fit at this position within the paratope, its further N-terminal extension as part of a polypeptide would lead to a steric clash.

The antigen-binding site of the Fab 2.2 with the bound P/A#1 epitope peptide forms a pronounced pocket to accommodate the central region of the peptide ligand with an ASA of 521 $Å^2$ buried, a value in a similar range as the peptide complexes described above. The three N-terminal peptide

residues form contacts with light chain CDRs only, while the C-terminal part is predominantly bound by the heavy chain CDRs. The main chain peptide groups give rise to five hydrogen bonds with residues located in CDRs H2, H3 and L3 (**Table S2**). Tyr^{L98} deserves special mention in this context as it acts as a hydrogen bond donor with its side chain hydroxyl group (to the oxygen atom of the N-terminal acetyl group of the P/A#1 peptide) and as a hydrogen bond acceptor with its main chain carbonyl oxygen (from the amide hydrogen of Ala^{P3}). On the side of the peptide, two Pro residues play an important role for the interaction with the Fab: Pro^{P2} is bound in a hydrophobic cage (Figure 4(E)) formed by three Tyr residues, Tyr^{L31} and Tyr^{L38} in CDR-L1 as well as Tyr^{L98} in CDR-L3, whereas Pro^{P7} is sandwiched between Asp^{H104} (CDR-H3) and Tyr^{H60} (CDR-H2). Overall, the shape of the combining site allows tight interactions with six residues of the epitope peptide, positioning residue Ala^{P5} at its centre, whose side chain becomes entirely buried upon complex formation (Figure 4(C) and Table S4). Furthermore, the carbonyl oxygen of Ala^{P5} is involved in two hydrogen bonds with Asn^{H52} and Trp^{H54}, both within CDR-H2, which emphasizes the role of this central Ala residue as a hot spot for antibody interactions with the P/A#1 epitope.

In contrast, the structure of the Fab 3.1 in complex with the $(APSA)_3$ peptide reveals a furrowed paratope, with the epitope peptide bound in a curled fashion between V_H and V_L, involving residues from all three APSA repeats. This peculiar mode of interaction permits tight complex formation, involving 94% of all peptide atoms and burying 1009 $Å^2$ of the peptide ASA, which is by far the largest value amongst the four Fab complexes investigated here. This is achieved by an exceptionally short CDR-H3 (Figure 5(A)) comprising only three residues. As a consequence, a small hydrophobic pocket is formed between CDR-H1 and CDR-H3, which perfectly accommodates residue Pro^{P3} of the peptide, thus providing a similar hydrophobic environment as the Tyr cage formed by the CDRs L1 and L3 in the structure of the Fab 2.2 in complex with the P/A#1 peptide described above. Furthermore, this allows the N-terminal half of the peptide to curl around the exposed hydrophobic side chain of Trp^{H99} (Figures 4(G) and (H)), which emerges as the key residue in the paratope by mediating 24% of all atom contacts with the peptide (Table S3). In addition, Trp^{H99} is involved in interactions with Pro^{P3} and Pro^{P7} where, if including the side chain of Tyr^{H27} on the other side of Pro^{P3}, in total four carbon rings are stacked in one line (Figure 4(G) and (H)). Similar to the other three Fab structures, six hydrogen bonds originating from the main chain peptide groups – including a bifurcated hydrogen bond between the Ala^{P6} amide and the Arg^{L51} guanidinium group (Figure 4(H)) – as well as two from Ser hydroxyl side chains stabilize the complex. Finally, there are local hydrophobic contacts with several peptide Pro and Ala side chains. Unlike the Fab structures 1.1 and 2.2, there is no pronounced pocket for a single Ala side chain in the paratope; yet, several Ala residues in the $(APSA)_3$ epitope play important roles in mediating hydrogen bonds and Van-der-Waals interactions (Tables S2 and S3).

To elucidate potential conformational similarities between the bound PAS#1 peptides in the complexes with the Fabs 1.1 and 1.2, a superposition between their structures was performed (Figure 5(B)). Interestingly, the four residues Ser^{P5} to Ala^{P8} showed a good match of their C_α positions, with a root mean square deviation (RMSD) of just 0.15 Å. Secondary structure analysis with STRIDE[32] identified a type I β-turn for this four-residue stretch. Apart from the intramolecular hydrogen bond between the Ser^{P5} carbonyl oxygen and the Ala^{P8} amide hydrogen, this turn is stabilized by a hydrogen bond between the Ser^{P5} hydroxyl oxygen and the Ala^{P7} amide hydrogen (Figure 5(B)). This type of β-turn is classified as SPXX turn and occurs in gene regulatory proteins where it acts as DNA-binding motif.[33] However, despite their mutual similarity in the two Fab complexes, these turns are bound in different orientations: in the complex with the Fab 1.1 this peptide moiety nestles into the binding pocket of the paratope, whereas it is exposed to the solvent in the complex with the Fab 1.2 (Figure 5(C) and (D)). Whether this turn represents a local low energy conformation only in the complex state or may also prevail in a free PAS (poly)peptide in solution remains elusive. However, one would expect a much higher antibody affinity, at least for the Fab, in case of a preformed rigid epitope conformation. On the other hand, the experimentally observed strongly expanded hydrodynamic volume of PAS polypeptides in solution[17] suggests high conformational flexibility along the entire amino acid chain. Furthermore, no defined secondary structure elements were detectable for the P/A#1 epitope peptide in the complex with the Fab 2.2 or for the $(APSA)_3$ peptide in complex with the Fab 3.1.

Discussion

In this study, we generated MAbs that specifically recognize linear epitopes in structurally disordered PAS (poly)peptides with three different sequences. Such MAbs, or their recombinant versions and fragments, offer valuable bioanalytical and diagnostic tools for the biochemical research as well as biopharmaceutical development of PASylated drug candidates,[18,23,34] including bioassays for clinical studies.

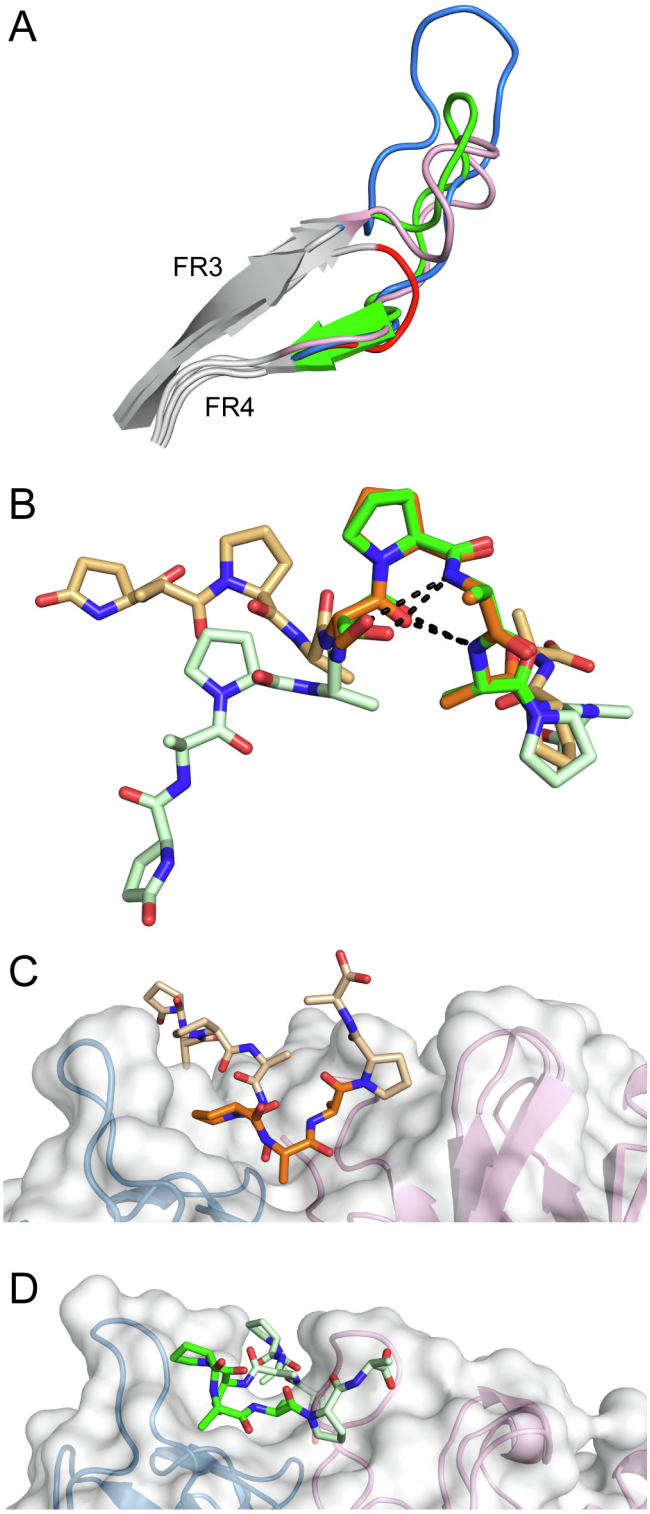

Figure 5. Structural details of the anti-PAS Fab•peptide complexes. (A) Superposition of the CDR-H3 hairpin loops of anti-PAS Fabs 1.1 (light pink), 1.2 (blue), 2.2 (green) and 3.1 (red), illustrating the extremely short CDR-H3 of Fab 3.1. (B) Superposition of the PAS#1 epitope peptide which adopts a type I β-turn in the complexes with both Fabs 1.1 (shades of orange) and 1.2 (shades of green). The peptides were aligned via the C_α atoms of residues Ser^{P5} to Ala^{P8} (RMSD = 0.15 Å). Intramolecular hydrogen bonds are shown as black dashed lines. (C and D) Differing orientations of the bound PAS#1 epitope peptide in the complexes with Fab 1.1 (C) and Fab 1.2 (D).

Despite elevated effort to raise these MAbs, involving relatively high antigen doses of PAS peptide conjugates with a strongly immunogenic carrier protein, extended boosting schemes and immunization of 5 animals per antigen, only a few independent hybridoma clones secreting IgG antibodies with decent binding activity were identified. Notably, low affinities in the nM range were only measurable for the MAbs with long PAS chains exhibiting multiple copies of the epitope sequence, obviously owing to the avidity effect. When the corresponding monovalent Fab fragments were tested, the dissociation constants were much higher, up to the μM range (see Table 1). Taken together, these findings indicate that structurally disordered PAS polypeptides represent poor immunogens and, if formed during an immune response, cognate IgG antibodies show poor to moderate affinities at best. This is in line with numerous animal studies that have been conducted with PASylated proteins so far, including repeated dosing in monkeys, where no immune response against the PAS moiety was evident.[20,21,24,35]

Nevertheless, the small set of viable MAbs that emerged from the present endeavour allowed functional studies as well as structural investigation of the corresponding recombinant Fab fragments. In general, antigen affinity was higher for the P/A#1 and APSA sequences than for PAS#1. One simple explanation may be twice the number of linear epitopes within the P/A#1 sequence repeat seen for the MAbs 2.1 and 2.2 (cf. Figure 1(A)) and even higher epitope density in the APSA sequence due to the short repetitive four-residue motif. Furthermore, the presence of Ser residues in the PAS#1 sequence[16] makes this prototypic PAS biopolymer slightly more hydrophilic than the P/A#1 polypeptide.[17] The latter sequence carries no polar side chains at all, whereas its favourable interaction with the aqueous solvent is dominated by the many hydrogen bond donors and acceptors in the polypeptide backbone that get fully exposed due to the absence of detectable secondary structure.

Our crystallographic studies of in total four different anti-PAS Fabs shed light on the mechanisms of molecular recognition of such low-complexity IDP sequences. Interestingly, the relative orientation of each epitope peptide within the antigen-binding site varies among these Fab complexes. The PAS#1 and $(APSA)_3$ peptides are oriented along the interface between V_H and V_L in the Fabs 1.1, 1.2 and 3.1, whereas the P/A#1 peptide in complex with the Fab 2.2 is bound across the V_L/V_H interface (see Figure 3(B)).

The loss of conformational entropy upon complex formation generally lowers the free energy of binding between conformationally disordered peptides and folded proteins, including antibodies. A comprehensive structural analysis using a database of high-resolution structures of peptide-protein complexes revealed that peptides are often bound such that changes in the three-dimensional structure of the binding protein are minimized, while on the other hand the enthalpy gain through Van der Waals packing and hydrogen bonding is maximized.[14] Indeed, the structure of the Fab 2.2 in complex with the P/A#1 epitope peptide illustrates a binding mechanism that was described to be typical for disordered antigens:[12] the peptide binds deeply within a concave paratope and buries a large proportion of its residues (75% of the ASA of the six central epitope residues on average; cf. Table S4). This notion is further supported by the structure of the Fab 3.1 in complex with the $(APSA)_3$ peptide, with 68% of the total peptide ASA buried in a distinct furrow of the paratope.

Comparison of the amino acid sequences of the variable domains of the different anti-PAS MAbs (see Figure 2) shows that there is high sequence similarity between MAbs raised against the same antigen: MAbs 1.1 and 1.2 with 88% identity for V_L, MAbs 2.1 and 2.2 with 87% amino acid identity for V_H and 94% for V_L, and MAbs 3.1 and 3.2 with 89% identity for V_H as well as V_L. This indicates the use of related germline genes, which were identified in an IMGT[36] database search (Table S5), revealing the same light and heavy chain V-gene families for MAbs 2.1 and 2.2 as well as 3.1 and 3.2, respectively. In contrast, the V_H sequences of MAbs 1.1 and 1.2 show a lower sequence identity of 53%, in agreement with different germline V-genes, IGHV2-6-7 and IGHV5-6-3, respectively. On the other hand, the fact that certain amino acid positions are functionally conserved between related MAbs is nicely illustrated for the light chain CDR residues Tyr^{L34} and Tyr^{L36} of MAbs 1.1 and 1.2. In both crystallized complexes, Tyr^{L34} forms a hydrophobic contact with the peptide residue Ala^{P2} while Tyr^{L36} is engaged in a hydrogen bond with the carbonyl oxygen of Pro^{P3}. Among the four crystallized Fabs, in total 66 contact residues were identified in the paratopes (Table S3) of which only 13 are not derived from germline sequences (Figure 2). Interestingly, all Trp contact residues are germline encoded (V or D). Also, all contact residues of Fab 1.2 correspond to germline sequences. Overall, this suggests a limitation in the number of ways how antibodies can recognize the feature-less PAS sequences, which may provide a structural explanation for their poor immunogenicity.

In all crystallized complexes of the anti-PAS Fab fragments, a high abundance of Tyr residues in the paratope is evident. These residues are responsible for the majority of hydrophobic contacts with the bound peptides (Table S3), thus creating surfaces well suited to bind antigens poor in charge or polar side chains. In fact, 62%, 49%, 43% and 23% of all contacts $\leq$4.0 Å are mediated

by Tyr in the MAbs 2.2, 1.2, 1.1 and 3.1, respectively. Interestingly, the Fab 2.2 revealed the highest Tyr content and also showed a comparably high affinity. This observation is in line with previous analyses suggesting that a high prevalence of Tyr in antibody paratopes generally contributes to enhanced antigen specificity and affinity.[19,37–39] Notably, a high proportion of Trp and Tyr was also reported for two murine anti-PEG antibodies whose crystal structures were recently published.[40,41] However, in both cases a peculiar ternary association mode was observed, involving two Fabs that bind face to face to the same region of one flexible PEG molecule.

Furthermore, in one of these studies the paratope seemed to give rise to a kind of dynamic ring structure which can capture PEG by wrapping around an exposed Trp side chain.[41] Hence, the structural mechanisms of binding a conformationally disordered polymer chain by antibodies share only remote resemblance between PEG and PAS antigens. A sequence alignment between the anti-PAS MAbs and the published anti-PEG antibodies 3.3, 2B5 and 6-3[40,41] did not reveal any particular similarities; neither could we identify a preference for germline genes. The only noticeable finding was a structurally equivalent position for Trp^{H99} (Kabat[28] position H95) in the anti-PAS Fab 3.1 when compared with the exposed Trp side chain at Kabat position H96 in the anti-PEG Fab 6-3 mentioned above (Figure S7), which might be caused by the short CDR-H3 in both antibodies (with three and five residues, respectively). Advances in the understanding of how antibodies can bind highly dynamic polymers such as PEG or PAS is of interest not only in the development of biopharmaceuticals with extended half-life but also in the context of COVID-19 vaccination. The two approved COVID-19 mRNA vaccines from Pfizer/BioNTech and Moderna both rely on PEGylated nanoparticles and clinical data have raised suspicions that the PEG moiety may be responsible for cases of anaphylactic shock in vaccine recipients, possibly after sensitization by PEG from cosmetics.[42,43]

Up to now, Ala, the amino acid with the smallest side chain – apart from the achiral Gly, which has no side chain at all – has been regarded to play a negligible role in protein–protein or -peptide recognition. In fact, the strategy of alanine-scanning mutagenesis[44] has found wide application to dissect critical residues for receptor-ligand or antibody-antigen binding,[45] assuming a quasi inert role of the methyl side chain for molecular interactions. Astonishingly, our studies have revealed for the first time that Ala actually can adopt a central role in epitope recognition by antibodies, as exemplified in particular with the crystal structures of the Fabs 1.1 and 2.2 in complex with a PAS#1 and a P/A#1 peptide, respectively. Fully buried in the binding pocket, and with its carbonyl oxygen involved in two hydrogen bonds, Ala^{P5} acts in fact as a kind of “hot spot” residue[46] at the centre of the antibody-peptide interface of the complex between Fab 2.2 and the P/A#1 epitope peptide (cf. Figure 4(C)). Even more strikingly, the structure of the Fab 1.1 reveals a pronounced hole in the middle of the antigen-binding site which is perfectly molded to accommodate the methyl group of Ala^{P7} within the PAS#1 epitope, resulting in high shape complementarity and a densely packed interface (cf. Figure 4(A)). A prominent role for Ala in molecular recognition is also reflected by the structure of the Fab 3.1 in complex with the $(APSA)_3$ peptide, where the three epitope residues Ala^{P6}, Ala^{P9} and Ala^{P10} are densely involved in interface formation and hydrogen bonding (Tables S2 and S4). Indeed, the SPOT substitution analysis experimentally supports the importance of these Ala residues, as binding decreased significantly when Ala was replaced by any other amino acid, even including Gly (Figure S5).

Our data offer insight into the mechanism of molecular recognition of structurally disordered peptide epitopes by antibodies. With no salt bridges and no pronounced hydrophobic side chain interactions arising from the PAS epitope in all of the assessed Fab structures, complex formation is mainly driven by hydrogen bonds involving the peptide backbone (Table S2) as well as tight Van der Waals contacts (Table S3, Figure 4(D) and (E)). It appears that due to the feature-less nature of the PAS peptides, the few atom groups in the antigen that are capable of polar interactions need to be capitalized by the antibody efficiently. The fact that at least four of the six CDRs are involved in the peptide-antibody interactions in all Fab complexes highlights the importance of an extended interface to more or less intimately bind the structurally flexible epitope. This is also nicely demonstrated by the structure of the Fab 1.2, where a short segment of the backbone hydrogen bond network with the PAS#1 peptide resembles an antiparallel β-sheet. Moreover, in both Fab complexes with the PAS#1 epitope peptide, comprising one prominent Ser residue, the antibody engages the only available polar side chain for formation of hydrogen bonds. The same is the case in the structure of the Fab 3.1, where two of the three Ser side chains are involved in hydrogen bonding. Notably, however, the MAbs 1.1 and 1.2 do not much functionally benefit from this kind of interaction if considering their significantly lower affinity compared with the anti-P/A#1 MAbs (see Table 1), which is in line with the expected limited energy gain of hydrogen bonds in a competing aqueous environment.[47,48]

In conclusion, by solving the complex structures of MAbs directed against different PAS sequences with their respective peptide antigens, our work sheds light onto how antibodies can bind to the seemingly inert PAS polypeptides with high specificity. These reagents, dubbed Avi-PA(S)™

MAbs, offer valuable tools for biomedical research as well as clinical application of PASylated proteins and peptides exerting pharmacological activity.

Materials & Methods

Preparation of PAS peptide conjugates for immunization

Three different peptides were obtained by solid phase synthesis (Peptide Specialty Laboratories – PSL, Heidelberg, Germany and Almac Sciences, Edinburgh, Scotland): Pga-PAS#1(40)-Ahx (Pga-ASPAAPAPASPAAPAPSAPAASPAAPAPASPAAPAPSAPA-Ahx); Pga-P/A#1(40)-Ahx (Pga-AAPAAPAPAAPAAPAPAAPAAPAPAAPAAPAPAA-Ahx); Pga-APSA(40)-Ahx (Pga-APSAAPSAAPSAAPSAAPSAAPSAAPSAAPSAAPSA-Ahx). As all peptides contained only chemically inert side chains and had a blocked N-terminus (Pga: pyroglutamyl), their unique C-terminal carboxylate groups (at the end of an aminohexanoic acid spacer, Ahx) were selectively activated and used for directed chemical conjugation with the ε-amino groups of Lys side chains of KLH, which was employed as a highly immunogenic carrier protein. To this end, 50 mg of each peptide was dissolved in 1450 μl dimethylsulfoxide (DMSO) and activated with a 10fold molar amount of each 2-(1H-benzotriazole-1-yl)-1,1,3,3-tetramethylaminium tetrafluoroborate (TBTU; Iris Biotech, Marktredwitz, Germany) and N,N-diisopropylethylamine (DIPEA; Sigma-Aldrich, Taufkirchen, Germany). 10 mg KLH (Thermo Fisher Scientific, Munich, Germany) was dissolved in water, dialyzed against PBS (4 mM KH_2PO_4, 16 mM Na_2HPO_4, 115 mM NaCl), adjusted to a concentration of 2.3 mg/ml in a volume of 4.35 ml and mixed with the activated peptide solution. After incubation on ice for 30 min, the solution was dialyzed against 25 mM Na-borate pH 9.0 and the conjugate was purified by anion exchange chromatography (AEX) on a Source 15Q column (GE Healthcare, Munich, Germany) equilibrated with the same buffer. The conjugate was eluted in a linear concentration gradient of 0–500 mM NaCl in running buffer (monitored at 280 nm). Eluate fractions of the main peak were pooled, dialyzed against PBS, concentrated to 2 mg/ml, sterile-filtered through a 0.22 μm Millex-GV PVDF filter (Merck, Darmstadt, Germany) and flash-frozen in liquid nitrogen.

Immunization of mice and generation of hybridoma cells

Using the PAS peptide-KLH conjugates described above as antigens, BALB/c mice were immunized and hybridomas were prepared according to standard procedures (ProMab Biotechnologies, Richmond, CA). For each antigen, five mice were immunized subcutaneously with 50 μg antigen together with Freund´s complete adjuvant (CFA). Three weeks after priming, three booster injections (five for APSA(40)-KLH), each with 25 μg antigen and Freund´s incomplete adjuvant, were applied at intervals of two weeks. A final boost with 50 μg of antigen without adjuvant was administered intraperitoneally two weeks after the last boost. Spleen cells were harvested from animals and fused with Sp2/0 myeloma cells for hybridoma clone generation.[49]

Characterization of antibodies from hybridoma cell culture supernatants via SPR and ELISA

IgG isotypes were determined by ProMab Biotechnologies using the mouse MoAb ID KIT (Zymed Laboratories, San Diego, CA). Promising hybridoma clones were cultivated in DMEM (Biochrom, Berlin, Germany) containing 10% v/v FCS (Ultra low IgG One Shot; Life Technologies, Carlsbad, CA), 6 mM L-alanyl-L-glutamine (Biochrom), 1:100 penicillin/streptomycin (Biochrom), further supplemented with 10% v/v Hybridoma Premium Medium (ProMab Biotechnologies), at 37 °C and under 5% CO_2 atmosphere. After initial screen by ELISA (see text), promising secreted anti-PAS MAbs in the hybridoma culture supernatants were characterized by real-time SPR spectroscopy and ELISA.

SPR measurements were performed at 25 °C either on a Biacore X100 or on a Biacore T200 instrument (GE Healthcare) using a Mouse Antibody Capture Kit and CM3 sensor chips (GE Healthcare). Hybridoma culture supernatants were diluted 1:5 in HBS-ET buffer (0.01 M HEPES/NaOH pH 7.4, 0.15 M NaCl, 3 mM EDTA, 0.005% v/v Tween20), and a 30 μl MAb sample was injected at a flow rate of 10 μl/min. A concentration series of the following test antigens, as appropriate, was then injected onto the sensor ship at a flow rate of 30 μl/min using single cycle kinetics:[50] PAS#1(200)-IL1Ra, P/A#1(200)-IL1Ra, P/A#1(600)-GMCSF, APSA(200)-IL1Ra and hu4D5-P/A#1(200).[16,17] The sensor chip was regenerated with 10 mM Gly/HCl pH 1.7 for 100 s. Data were analyzed using the Biacore X100 evaluation software ver. 2.0.1 (GE Healthcare) with a bivalent analyte fit after subtraction of signals from both a reference channel and a blank baseline measured with HBS-ET buffer.

Characterization of MAbs by ELISA was performed using NUNC Maxisorp F 96-well plates (Thermo Fisher Scientific) coated with 50 μl of a 5 μg/ml solution of anti-mouse IgG Fc-specific goat antibody (Sigma-Aldrich) in PBS for 1 h, followed by twice washing with PBS and blocking with 3% w/v bovine serum albumin (BSA) in PBS/T (PBS containing 0.1% v/v Tween 20) for 1 h. After washing with PBS/T, the wells were

incubated for 1 h with 50 µl of each hybridoma culture supernatant diluted 1:100 in PBS/T and washed again. Then, 50 µl solutions of the following PASylated proteins (each 8 nM) were applied in 1:2 dilution series with PBS/T and incubated for 1 h: hu4D5-PAS#1(200), hu4D5-P/A#1(200) or APSA(200)-IL1Ra, the latter labeled with DIG-NHS (Santa Cruz Biotechnology, Dallas, TX) according to the manufacturer's instructions. After washing with PBS/T, 50 µl of a 1:1000 dilution of anti-human kappa light chain antibody alkaline phosphatase conjugate (Sigma-Aldrich) or anti-DIG-Fab alkaline phosphatase conjugate (Roche Diagnostics, Mannheim, Germany), respectively, was applied to each well and incubated for 1 h. After final washing with PBS, 50 µl of 0.5 mg/ml *p*-nitrophenyl phosphate (Merck) in AP buffer (100 mM Tris/HCl pH 8.8, 100 mM NaCl, 5 mM $MgCl_2$) was added and signal development was recorded at 405 nm for 15 min at 1 min intervals using a Synergy 2 photometer (BioTek Instruments, Bad Friedrichshall, Germany). The concentration-dependent signals ($\Delta A/\Delta t$) were evaluated using the Voss&Skerra equation.[51]

Cloning of V-genes from hybridomas

Hybridoma cells were mechanically lysed and total RNA was extracted using the RNeasy Mini Kit (Qiagen, Hilden, Germany), followed by cDNA synthesis using the First Strand cDNA Synthesis Kit (Thermo Fisher Scientific) with an oligo$(dT)_{18}$ primer. Ig V-gene regions were PCR-amplified from this cDNA with Q5 DNA polymerase (New England Biolabs, Frankfurt/M. Germany) using a set of 63 forward primers covering all mouse germline V_L/V_H gene segments[52] together with the reverse primers RMK (5′-GAC CTC CAC GGA GTC AGC-3′) for the light chain and RMG (5′-AGG TCG CCA CAC GTG TGG-3′) for the heavy chain.[53] Forward primers were initially applied in pools of 5–15 different oligodeoxynucleotides, in order to reduce the required number of PCRs, and then individually, after an amplification product was identified, to generate a homogenous PCR product. DNA fragments with suitable size were isolated after separation by agarose gel electrophoresis using the Wizard SV Gel and PCR Clean-Up System (Promega, Madison, WI) and subjected to double-stranded DNA sequencing using the Mix2-Seq Kit (Eurofins Genomics, Ebersberg, Germany).

Construction of bacterial expression plasmids for Fab fragments

For cloning of the V-genes on the bacterial expression vector pASK88,[29] the products from the V-gene amplification described above were PCR-amplified with primer pairs that were designed to introduce suitable flanking restriction sites according to a published procedure.[53,54] The resulting PCR products were cut with the corresponding restriction enzymes, isolated by agarose gel electrophoresis, and the V_H and V_L genes were inserted into the appropriately digested pASK88 in two consecutive ligations. The coding regions for the MAbs 1.2, 2.1 and 3.1 were obtained by gene synthesis with optimized *E. coli* codon usage and suitable flanking restriction sites (Thermo Fisher Scientific) based on V-gene sequences determined by ProMab Biotechnologies.

E. coli production and purification of Fab fragments

pASK88 derivatives harbouring the corresponding V-genes were used to express the chimeric Fab fragments (i.e., murine variable domains from the hybridomas fused to human constant domains) either in 2 l shake flask cultures using *E. coli* strain JM83[55] or via 8 l bench top fermentation using the strain KS272[56] following published procedures.[29,30] The recombinant proteins were purified from the periplasmic cell extract via immobilized metal ion affinity chromatography (IMAC), followed by cation exchange chromatography (CEX) on a Resource S 6 ml column and by size exclusion chromatography (SEC) on a HiLoad 16/60 Superdex75 prep grade column (both from GE Healthcare). Protein concentrations were determined by measuring the absorbance at 280 nm using calculated extinction coefficients[57] of 77405 M^{-1} cm^{-1}, 66405 M^{-1} cm^{-1}, 88405 M^{-1} cm^{-1}, 89895 M^{-1} cm^{-1}, 69955 M^{-1} cm^{-1} or 57465 M^{-1} cm^{-1} for the chimeric Fab fragments 1.1, 1.2, 2.1, 2.2, 3.1 or 3.2, respectively. Protein integrity and purity were checked by SDS-PAGE[58] and by electrospray ionization mass spectrometry (ESI-MS) using a maXis Q-TOF instrument (Bruker Daltonics, Bremen, Germany) in the positive ion mode.

E. coli production and purification of the anti-human kappa light chain V_HH domain

A previous study had shown that an anti-human kappa V_HH domain may facilitate the (co)-crystallization of Fab fragments containing a human κ light chain.[31] Since the sequence information for the anti-huκ V_HH domain crystallized in complex with a Fab was missing in the PDB coordinate set 6ANA[31] the polypeptide chain SEQ ID NO: 1 from a patent publication[59] was fitted into the well-defined electron density calculated from the deposited structure factors using Coot.[60] The corresponding coding region was generated by gene synthesis (Eurofins Genomics) and cloned via *Xba*I and *Hin*dIII on the generic expression vector pASK75[61] in frame with a C-terminal His_6-tag. The V_HH domain was produced in shake flask culture using the *E. coli* strain Origami B[62] grown at 30 °C in LB medium[49] supplemented with 100 mg/l ampicillin. Gene expression was induced at OD_{550} = 0.5 for

3 h by adding anhydrotetracycline (Acros Organics, Geel, Belgium) to a final concentration of 0.2 μg/ml. After centrifugation, the bacterial pellet was resuspended in IMAC buffer (50 mM Tris/HCl pH 8, 300 mM NaCl), which was supplemented with 10 mM 2,2-dithiodipyridine (Sigma-Aldrich) to promote quantitative formation of the intramolecular disulphide bond, and the bacteria were lysed using a French pressure cell (SLM Aminco, Urbana, IL). The whole cell lysate was clarified by centrifugation and the supernatant was subjected to IMAC using a 5 ml HisTrap HP column (GE Healthcare). The recombinant protein was eluted using a concentration gradient of 0–300 mM imidazole/HCl in IMAC running buffer. Eluted protein fractions were identified by SDS-PAGE, pooled and dialyzed twice against CEX buffer (50 mM Na-acetate pH 5.5, 20 mM NaCl). The protein solution was then applied to a 6 ml Resource S column (GE Healthcare) and the anti-huκ V_HH domain was eluted in a linear concentration gradient of 0–250 mM NaCl in CEX buffer. Finally, fractions containing the protein were concentrated and applied to a HiLoad 16/60 Superdex75 prep grade column (GE Healthcare) pre-equilibrated with IMAC buffer. Protein purity was checked by SDS-PAGE and ESI-MS as above using a calculated extinction coefficient of 23045 M^{-1} cm^{-1}.

Antigen affinity measurements by ELISA and SPR

A NUNC Maxisorp F 96-well plate was coated with 50 μl of 10 μg/ml P/A#1(600) polypeptide[17] in PBS for the Fabs 2.1 and 2.2, with 50 μl of 10 μg/ml PAS#1(600)-Leptin[63] in PBS for the Fabs 1.1 and 1.2, or with 50 μl of 10 μg/ml APSA(200)-IL1Ra[17] for the Fabs 3.1 and 3.2 and incubated at 4 °C overnight. After washing with PBS/T, the wells were blocked with 3% w/v BSA (NeoFROXX, Einhausen, Germany) in PBS/T for 1 h, followed by 3x washing and 1 h incubation with 50 μl of an appropriate dilution series of each purified Fab fragment in PBS/T. The wells were washed again with PBS/T, followed by incubation with 50 μl of a 1:1000 dilution of anti-human kappa light chain goat antibody conjugated to alkaline phosphatase (Sigma-Aldrich) in PBS/T for 1 h. After final washing twice each with PBS/T and PBS, signals were developed with *p*-nitrophenyl phosphate and measured and evaluated as described above.

SPR measurements with the purified Fab fragments were performed on a Biacore X100 instrument (GE Healthcare) at 25 °C. PAS#1(200)-IL1Ra, P/A#1(200)-IL1Ra or thioredoxin A (TrxA)-APSA(200) were biotinylated with a 20-fold molar amount of succinimidyl-6-(biotinamido) hexanoate (Sigma Aldrich) and individually immobilized as ligands on a biotin CAPture chip (GE Healthcare) according to the manufacturer´s protocol. Prior to immobilisation of the ligand protein, the sensorchip was regenerated with two consecutive injections of 30% v/v acetonitrile, 0.25 M NaOH for 120 s as well as 6 M guanidine/HCl, 0.25 M NaOH for 120 s. Subsequently, a concentration series of the recombinant Fab fragment was injected as analyte onto the sensorchip at a flow rate of 30 μl/min using single cycle kinetics. After subtraction of signals from both a reference channel and a blank baseline measured with HBS-ET buffer, data were fitted using the Biacore X100 evaluation software ver. 2.0.1 (GE Healthcare) using a 1:1 binding model. The equilibrium dissociation constant was calculated as $K_D = k_{off} / k_{on}$, whereby its statistical error was calculated from the standard deviations of the individual kinetic constants as described.[64]

SPOT synthesis of immobilized peptide arrays and epitope mapping

Arrays of 20 overlapping 12mer peptides covering the entire amino acid sequence of the PAS#1 or P/A#1 amino acid sequence repeat, or of a 10mer peptide comprising the sequence AAPSAAPSAA, including substitution by all 20 proteinogenic amino acids at positions 3 to 8, were synthesized on a hydrophilic membrane using a MultiPep SPOT synthesizer (Intavis, Köln, Germany) according to a standard protocol.[27] Detection of antibody binding activity on the membranes was performed using a published procedure[65] after incubation with either the purified Fab fragment (applied at 1 μg/ml in MBS; 137 mM NaCl, 2.7 mM KCl, 50 mM Tris/HCl pH 8, 0.05% v/v Tween-20, 1% w/v sucrose) or the hybridoma culture supernatant containing the secreted MAb (diluted 1:5000 in MBS), followed by an anti-human kappa light chain antibody alkaline phosphatase conjugate (Sigma-Aldrich) or anti-mouse IgG Fc-specific goat antibody alkaline phosphatase conjugate (Sigma-Aldrich), respectively. After chromogenic reaction, the spot intensities were quantified with CLIQS ver. 1.2.044 software (TotalLab, Newcastle-upon-Tyne, UK).

Detection of PASylated proteins by western blotting

To test hybridoma culture supernatants for detection of PASylated proteins on western blots, a set of different PASylated proteins, PAS#1(200)-IL1Ra, P/A#1(200)-IL1Ra and APSA(200)-IL1Ra, was subjected to SDS-PAGE, followed by semi-dry electrotransfer onto a nitrocellulose membrane. An *E. coli* BL21 whole cell lysate and human serum (PL), pooled (SEQENS IVD / H2B, Limoges, France), which was diluted 1:200 in water and spiked with 1 μg IL-1Ra (Anakinra/Kineret®; Swedish Orphan Biovitrum, Stockholm, Sweden), were applied in parallel as controls. After washing with PBS/T, the membrane was incubated with a 1:2000 dilution in PBS/T of the hybridoma culture supernatants or a 1:200.000

dilution of the purified MAb 2.1. Bound MAbs were detected using a 1:50.000 dilution of an anti-mouse IgG Fc-specific goat antibody conjugated with alkaline phosphatase in PBS/T followed by chromogenic reaction as above.

Co-crystallization of Fab fragments with PAS peptides, X-ray data collection and model building

The purified recombinant Fab fragments 1.1, 2.2 and 3.1 were directly co-crystallized with their cognate PAS epitope peptides, whereas in the case of Fab 1.2 a complex with an anti-huκ V_HH domain was prepared. To this end, the purified Fab was incubated for 1 h at 4 °C with a three-fold molar amount of the purified V_HH domain from above. The protein mixture was subjected to SEC on a HiLoad 16/60 Superdex75 prep grade column using 10 mM HEPES/NaOH pH 6.5, 70 mM NaCl as running buffer, and the Fab•V_HH complex was separated from excess V_HH domain and isolated in one peak.

The different Fab solutions were concentrated using Amicon Ultracel centrifugal filter units (MWCO 10 kDa; Millipore, Billerica, MA) as follows: Fab 1.1 at 8.4 mg/ml and Fab 1.2 in complex with V_HH at 13.7 mg/ml, both in 10 mM HEPES/NaOH pH 6.5, 70 mM NaCl; Fab 2.2 at 9.6 mg/ml in 20 mM HEPES/NaOH pH 6.5, 80 mM NaCl; Fab 3.1 at 9.2 mg/ml in 10 mM HEPES, pH 6.5, 100 mM NaCl. Each concentrated protein solution was mixed with the appropriate synthetic peptide from a > 50 mM stock solution in water (see Table S1) at a molar ratio of 1:3 (Fab:peptide) and incubated for 1 h at 4 °C. Subsequently, protein crystallization screens were performed via the sitting drop vapour diffusion method with equal volumes of protein and reservoir solutions, leading to a total drop volume in the range of 300–1000 nl, using an in-house precipitant screen. For refinement of promising crystallization conditions, further screens were set up using the hanging drop vapour diffusion method with a reservoir volume of 1 ml and droplets composed of 1 μl protein and 1 μl reservoir solutions. Crystals appeared within one week at 20 °C under the conditions listed in Table S1. Protein crystals were harvested, transferred into the precipitant buffer supplemented with 20% v/v ethylene glycol for Fab 1.1 and Fab 1.2, 20% w/v PEG200 for Fab 2.2 and 20% v/v glycerol for Fab 3.1, and immediately frozen in liquid nitrogen.

For each crystal of the Fabs 1.1, 1.2 and 2.2, a single-wavelength synchrotron X-ray cryo-diffraction data set was collected at BESSY beamline 14.2 operated by the Helmholtz-Zentrum Berlin, Germany.[66] In case of the Fab 3.1, the protein crystallography beamline X06SA-PXI at the Swiss Light Source (SLS), Villigen-PSI, Switzerland, was used. The diffraction data (Table S1) were reduced and scaled with the XDS program package,[67] and molecular replacement was carried out with Phaser[68] using the constant and variable domains of the functionally unrelated anti-human RSV Fab 101F (PDB ID: 3QQ9), which shares similarity in the amino acid sequence, as search models to first solve the structure of the Fab 2.2 in complex with the P/A#1 epitope peptide. The structures of Fab 1.1 and Fab 1.2, both with the bound PAS#1 epitope peptide, were subsequently solved by molecular replacement with the refined crystal structure of the Fab 2.2 as search model, additionally including coordinates for the anti-huκ V_HH domain (PDB ID: 6ANA) in the latter case. Finally, the structure of Fab 3.1 in complex with the $(APSA)_3$ peptide was solved by molecular replacement using the refined structure of Fab 1.2 as search model.

The initial protein models were manually adjusted with Coot[60] and iteratively refined with Refmac5.[69] The PAS#1, P/A#1 and $(APSA)_3$ epitope peptides and water molecules were manually built into emerging electron densities in the course of the refinement process. The final structural models, showing R_{free} values of 23–27% (Table S1), were validated using the MolProbity server.[70] Crystal contact sites as well as accessible and buried surface areas (ASA and BSA, respectively; calculated with the light and heavy chains renumbered as a continuous amino acid chain in the input file to ensure proper calculation) were analysed with PISA.[71] Molecular graphics were prepared with PyMOL (Schrödinger, Cambridge, MA) using the APBS module[72] for calculation of electrostatics. Atomic distances were calculated with CONTACT.[73]

Polypeptides were denoted L for each Ig light chain, H for each heavy chain and P for each bound PAS peptide whereas the anti-human kappa V_HH domain was assigned the chain identifier X. In case of the Fab 1.1 with two Fab•peptide complexes in the asymmetric unit the one with the higher average crystallographic B-factor was assigned chain identifiers A, B and Q, respectively. The atom coordinates and structure factors of the four refined crystal structures have been deposited at the Protein Data Bank (PDB), Research Collaboratory for Structural Bioinformatics (Rutgers University, New Brunswick, NJ), under accession codes 7O30 (Fab 1.1), 7O31 (Fab 1.2), 7O2Z (Fab 2.2) and 7O33 (Fab 3.1).

Accession numbers

PDB: 7O30, 7O31, 7O2Z, 7O33.

CRediT authorship contribution statement

J. Schilz: Investigation, Visualization, Writing - original draft, Writing - review & editing. **U.**

Binder: Conceptualization, Investigation, Writing - review & editing. **L. Friedrich:** Resources, Writing - review & editing. **M. Gebauer:** Resources, Writing - review & editing. **C. Lutz:** Resources, Writing - review & editing. **M. Schlapschy:** Investigation, Writing - review & editing. **A. Schiefner:** Investigation, Writing - review & editing. **A. Skerra:** Conceptualization, Supervision, Writing - original draft, Writing - review & editing.

Acknowledgement

The authors wish to thank Klaus Wachinger (TUM) for assistance with fermentation of *E. coli*, Dr. Hyun-Jin Kim (XL-protein) for help in some ELISAs, Stefan Achatz (TUM) for ESI-MS and Dr. Andreas Eichinger, Dr. Eva Huber and Prof. Dr. Michael Groll (all at TUM) for crystallographic data collection. The authors are grateful to the Helmholtz-Zentrum Berlin, Germany, for allocation of synchrotron radiation beamtime and travel support and Dr. Thomas Hauß for technical support at BESSY beamline 14.2 as well as Dr. John Henry Beale for technical support at SLS beamline X06SA-PXI.

Declaration of Competing Interest

A.Sk., M.S. and U.B. are shareholders of XL-protein GmbH. The other authors declare that they have no known competing financial interests or personal relationships that could have appeared to influence the work reported in this paper.

Appendix A. Supplementary material

Supplementary data to this article can be found online at https://doi.org/10.1016/j.jmb.2021.167113.

Received 26 April 2021;
Accepted 15 June 2021;
Available online 20 June 2021

Keywords:
Avi-PA(S) MAb;
disordered antigen;
intrinsically disordered protein;
natively unfolded protein;
PASylation

References

1. Wright, P.E., Dyson, H.J., (2015). Intrinsically disordered proteins in cellular signalling and regulation. *Nat. Rev. Mol. Cell Biol.*, **16**, 18–29.
2. Tantos, A., Han, K.H., Tompa, P., (2012). Intrinsic disorder in cell signaling and gene transcription. *Mol. Cell. Endocrinol.*, **348**, 457–465.
3. Snead, D., Eliezer, D., (2019). Intrinsically disordered proteins in synaptic vesicle trafficking and release. *J. Biol. Chem.*, **294**, 3325–3342.
4. Feng, Z.P., Zhang, X., Han, P., Arora, N., Anders, R.F., Norton, R.S., (2006). Abundance of intrinsically unstructured proteins in *P. falciparum* and other apicomplexan parasite proteomes. *Mol. Biochem. Parasitol.*, **150**, 256–267.
[5]. Goh, G.K., Dunker, A.K., Uversky, V.N., (2016). Correlating Flavivirus virulence and levels of intrinsic disorder in shell proteins: Protective roles vs. immune evasion. *Mol. BioSyst.*, **12**, 1881–1891.
6. Giri, R., Kumar, D., Sharma, N., Uversky, V.N., (2016). Intrinsically disordered side of the Zika virus proteome. *Front. Cell. Infect. Microbiol.*, **6**, 144.
7. Barlow, D.J., Edwards, M.S., Thornton, J.M., (1986). Continuous and discontinuous protein antigenic determinants. *Nature*, **322**, 747–748.
[8]. Huang, J., Honda, W., (2006). CED: A conformational epitope database. *BMC Immunol.*, **7**, 7.
9. Mészáros, B., Tompa, P., Simon, I., Dosztányi, Z., (2007). Molecular principles of the interactions of disordered proteins. *J. Mol. Biol.*, **372**, 549–561.
[10]. Fong, J.H., Shoemaker, B.A., Garbuzynskiy, S.O., Lobanov, M.Y., Galzitskaya, O.V., Panchenko, A.R., (2009). Intrinsic disorder in protein interactions: Insights from a comprehensive structural analysis. *PLoS Comput. Biol.*, **5**, e1000316
[11]. Uversky, V.N., (2019). Intrinsically disordered proteins and their “mysterious” (meta)physics. *Front. Phys.*, **7**, 10
12. MacRaild, C.A., Richards, J.S., Anders, R.F., Norton, R.S., (2016). Antibody recognition of disordered antigens. *Structure*, **24**, 148–157.
13. Fassolari, M., Chemes, L.B., Gallo, M., Smal, C., Sanchez, I.E., de Prat-Gay, G., (2013). Minute time scale prolyl isomerization governs antibody recognition of an intrinsically disordered immunodominant epitope. *J. Biol. Chem.*, **288**, 13110–13123.
14. London, N., Movshovitz-Attias, D., Schueler-Furman, O., (2010). The structural basis of peptide-protein binding strategies. *Structure*, **18**, 188–199.
15. Schellenberger, V., Wang, C.W., Geething, N.C., Spink, B. J., Campbell, A., To, W., et al., (2009). A recombinant polypeptide extends the *in vivo* half-life of peptides and proteins in a tunable manner. *Nat. Biotechnol.*, **27**, 1186–1190.
16. Schlapschy, M., Binder, U., Börger, C., Theobald, I., Wachinger, K., Kisling, S., et al., (2013). PASylation: a biological alternative to PEGylation for extending the plasma half-life of pharmaceutically active proteins. *Protein Eng. Des. Sel.*, **26**, 489–501.
[17]. Breibeck, J., Skerra, A., (2018). The polypeptide biophysics of proline/alanine-rich sequences (PAS): Recombinant biopolymers with PEG-like properties. *Biopolymers*, **109**, e23069
18. Binder, U., Skerra, A., (2017). PASylation®: A versatile technology to extend drug delivery. *Curr. Opin. Colloid Interface Sci.*, **31**, 10–17.
19. Wang, M., Zhu, D., Zhu, J., Nussinov, R., Ma, B., (2018). Local and global anatomy of antibody-protein antigen recognition. *J. Mol. Recognit.*, **31**, e2693

20. Bolze, F., Morath, V., Bast, A., Rink, N., Schlapschy, M., Mocek, S., et al., (2016). Long-acting PASylated leptin ameliorates obesity by promoting satiety and preventing hypometabolism in leptin-deficient $lep^{ob/ob}$ mice. *Endocrinology*, **157**, 233–244.
21. Harari, D., Kuhn, N., Abramovich, R., Sasson, K., Zozulya, A.L., Smith, P., et al., (2014). Enhanced *in vivo* efficacy of a type I interferon superagonist with extended plasma half-life in a mouse model of multiple sclerosis. *J. Biol. Chem.*, **289**, 29014–29029.
22. Mendler, C.T., Friedrich, L., Laitinen, I., Schlapschy, M., Schwaiger, M., Wester, H.J., et al., (2015). High contrast tumor imaging with radio-labeled antibody Fab fragments tailored for optimized pharmacokinetics via PASylation. *MAbs.*, **7**, 96–109.
23. Richter, A., Knorr, K., Schlapschy, M., Robu, S., Morath, V., Mendler, C., et al., (2020). First in-human medical imaging with a PASylated ^{89}Zr-labeled anti-HER2 Fab-fragment in a patient with metastatic breast cancer. *Nucl. Med. Mol. Imaging*, **54**, 114–119.
24. Griffiths, K., Binder, U., McDowell, W., Tommasi, R., Frigerio, M., Darby, W.G., et al., (2019). Half-life extension and non-human primate pharmacokinetic safety studies of i-body AD-114 targeting human CXCR4. *MAbs*, **11**, 1331–1340.
25. Swaminathan, A., Lucas, R.M., Dear, K., McMichael, A.J., (2014). Keyhole limpet haemocyanin – a model antigen for human immunotoxicological studies. *Br. J. Clin. Pharmacol.*, **78**, 1135–1142.
26. Köhler, G., Milstein, C., (1975). Continuous cultures of fused cells secreting antibody of predefined specificity. *Nature*, **256**, 495–497.
27. Frank, R., (2002). The SPOT-synthesis technique. Synthetic peptide arrays on membrane supports–principles and applications. *J. Immunol. Methods*, **267**, 13–26.
28. Kabat, E.A., Wu, T.T., Perry, H.M., Gottesman, K.S., Foeller, C., (1991). Sequences of Proteins of Immunological Interest. National Institute of Health, Bethesda, MD.
29. Schiweck, W., Skerra, A., (1995). Fermenter production of an artificial Fab fragment, rationally designed for the antigen cystatin, and its optimized crystallization through constant domain shuffling. *Proteins*, **23**, 561–565.
30. Skerra, A., (1994). A general vector, pASK84, for cloning, bacterial production, and single-step purification of antibody Fab fragments. *Gene*, **141**, 79–84.
31. Ereño-Orbea, J., Sicard, T., Cui, H., Carson, J., Hermans, P., Julien, J.P., (2018). Structural basis of enhanced crystallizability induced by a molecular chaperone for antibody antigen-binding fragments. *J. Mol. Biol.*, **430**, 322–336.
32. Frishman, D., Argos, P., (1995). Knowledge-based protein secondary structure assignment. *Proteins*, **23**, 566–579.
33. Suzuki, M., Yagi, N., (1991). Structure of the SPXX motif. *Proc. Biol. Sci.*, **246**, 231–235.
34. Gebauer, M., Skerra, A., (2018). Prospects of PASylation® for the design of protein and peptide therapeutics with extended half-life and enhanced action. *Bioorg. Med. Chem.*, **26**, 2882–2887.
35. Längin, M., Mayr, T., Reichart, B., Michel, S., Buchholz, S., Guethoff, S., et al., (2018). Consistent success in life-supporting porcine cardiac xenotransplantation. *Nature*, **564**, 430–433.
36. Brochet, X., Lefranc, M.P., Giudicelli, V., (2008). IMGT/V-QUEST: The highly customized and integrated system for IG and TR standardized V-J and V-D-J sequence analysis. *Nucleic Acids Res.*, **36**, W503–W508.
37. Birtalan, S., Zhang, Y., Fellouse, F.A., Shao, L., Schaefer, G., Sidhu, S.S., (2008). The intrinsic contributions of tyrosine, serine, glycine and arginine to the affinity and specificity of antibodies. *J. Mol. Biol.*, **377**, 1518–1528.
38. Birtalan, S., Fisher, R.D., Sidhu, S.S., (2010). The functional capacity of the natural amino acids for molecular recognition. *Mol. BioSyst.*, **6**, 1186–1194.
39. Peng, H.P., Lee, K.H., Jian, J.W., Yang, A.S., (2014). Origins of specificity and affinity in antibody-protein interactions. *Proc. Natl. Acad. Sci. USA*, **111**, E2656–E2665.
40. Lee, C.-C., Su, Y.-C., Ko, T.-P., Lin, L.-L., Yang, C.-Y., Chang, S.S.-C., et al., (2020). Structural basis of polyethylene glycol recognition by antibody. *J. Biomed. Sci.*, **27**, 12.
[41]. Huckaby, J.T., Jacobs, T.M., Li, Z., Perna, R.J., Wang, A., Nicely, N.I., et al., (2020). Structure of an anti-PEG antibody reveals an open ring that captures highly flexible PEG polymers. *Commun. Chem.*, **3**, 124.
42. Garvey, L.H., Nasser, S., (2021). Anaphylaxis to the first COVID-19 vaccine: Is polyethylene glycol (PEG) the culprit? *Br. J. Anaesth.*, **126**, e106–e108.
43. Moghimi, S.M., (2021). Allergic reactions and anaphylaxis to LNP-based COVID-19 vaccines. *Mol. Ther.*, **29**, 898–900.
44. Cunningham, B.C., Wells, J.A., (1989). High-resolution epitope mapping of hGH-receptor interactions by alanine-scanning mutagenesis. *Science*, **244**, 1081–1085.
45. Morrison, K.L., Weiss, G.A., (2001). Combinatorial alanine-scanning. *Curr. Opin. Chem. Biol.*, **5**, 302–307.
46. Clackson, T., Wells, J.A., (1995). A hot spot of binding energy in a hormone-receptor interface. *Science*, **267**, 383–386.
47. Fersht, A.R., (1987). The hydrogen bond in molecular recognition. *Trends Biochem. Sci.*, **12**, 301–304.
48. Gao, J., Bosco, D.A., Powers, E.T., Kelly, J.W., (2009). Localized thermodynamic coupling between hydrogen bonding and microenvironment polarity substantially stabilizes proteins. *Nat. Struct. Mol. Biol.*, **16**, 684–690.
49. Sambrook, J.F., Russell, D.W., (2001). Molecular Cloning: A Laboratory Manual. Cold Spring Harbor Laboratory Press, Cold Spring Harbor, N.Y..
50. Karlsson, R., Katsamba, P.S., Nordin, H., Pol, E., Myszka, D.G., (2006). Analyzing a kinetic titration series using affinity biosensors. *Anal. Biochem.*, **349**, 136–147.
51. Voss, S., Skerra, A., (1997). Mutagenesis of a flexible loop in streptavidin leads to higher affinity for the *Strep*-tag II peptide and improved performance in recombinant protein purification. *Protein Eng.*, **10**, 975–982.
52. Chardès, T., Villard, S., Ferrières, G., Piechaczyk, M., Cerutti, M., Devauchelle, G., et al., (1999). Efficient amplification and direct sequencing of mouse variable regions from any immunoglobulin gene family. *FEBS Lett.*, **452**, 386–394.
53. Loers, G., Cui, Y.F., Neumaier, I., Schachner, M., Skerra, A., (2014). A Fab fragment directed against the neural cell adhesion molecule L1 enhances functional recovery after injury of the adult mouse spinal cord. *Biochem. J.*, **460**, 437–446.

[54]. Peplau, E., De Rose, F., Reder, S., Mittelhaeuser, M., Scafetta, G., Schwaiger, M., et al., (2020). Development of a chimeric Fab directed against human galectin-3 and validation as an immune-PET tracer for the sensitive *in vivo* imaging of thyroid cancer. *Thyroid*, **30**, 1314–1326.
55. Yanisch-Perron, C., Vieira, J., Messing, J., (1985). Improved M13 phage cloning vectors and host strains: Nucleotide sequences of the M13mp18 and pUC19 vectors. *Gene*, **33**, 103–119.
56. Meerman, H.J., Georgiou, G., (1994). Construction and characterization of a set of *E. coli* strains deficient in all known loci affecting the proteolytic stability of secreted recombinant proteins. *Biotechnology (N Y)*, **12**, 1107–1110.
57. Gasteiger, E., Gattiker, A., Hoogland, C., Ivanyi, I., Appel, R.D., Bairoch, A., (2003). ExPASy: The proteomics server for in-depth protein knowledge and analysis. *Nucleic Acids Res.*, **31**, 3784–3788.
58. Fling, S.P., Gregerson, D.S., (1986). Peptide and protein molecular weight determination by electrophoresis using a high-molarity tris buffer system without urea. *Anal. Biochem.*, **155**, 83–88.
59. Hermans, W.J.J., Ten Haaft, M.R., Overweel, A., (2006). Method for affinity purification. *WO 2006/059904 A1*,.
60. Emsley, P., Lohkamp, B., Scott, W.G., Cowtan, K., (2010). Features and development of Coot. *Acta Crystallogr. D Biol. Crystallogr.*, **66**, 486–501.
61. Skerra, A., (1994). Use of the tetracycline promoter for the tightly regulated production of a murine antibody fragment in *Escherichia coli*. *Gene*, **151**, 131–135.
62. Bessette, P.H., Aslund, F., Beckwith, J., Georgiou, G., (1999). Efficient folding of proteins with multiple disulfide bonds in the *Escherichia coli* cytoplasm. *Proc. Natl. Acad. Sci. USA*, **96**, 13703–13708.
63. Morath, V., Bolze, F., Schlapschy, M., Schneider, S., Sedlmayer, F., Seyfarth, K., et al., (2015). PASylation of murine leptin leads to extended plasma half-life and enhanced *in vivo* efficacy. *Mol. Pharm.*, **12**, 1431–1442.
[64]. Schönfeld, D., Matschiner, G., Chatwell, L., Trentmann, S., Gille, H., Hülsmeyer, M., et al., (2009). An engineered lipocalin specific for CTLA-4 reveals a combining site with structural and conformational features similar to antibodies. *Proc. Natl. Acad. Sci. USA*, **106**, 8198–8203.
65. Zander, H., Reineke, U., Schneider-Mergener, J., Skerra, A., (2007). Epitope mapping of the neuronal growth inhibitor Nogo-A for the Nogo receptor and the cognate monoclonal antibody IN-1 by means of the SPOT technique. *J. Mol. Recognit.*, **20**, 185–196.
[66]. Gerlach, M., Mueller, U., Weiss, M.S., (2016). The MX beamlines BL14.1-3 at BESSY II. *J. Large-Scale Res. Fac.*, **2**, A47
67. Kabsch, W., (2010). XDS. *Acta Crystallogr. D Biol. Crystallogr.*, **66**, 125–132.
68. McCoy, A.J., Grosse-Kunstleve, R.W., Adams, P.D., Winn, M.D., Storoni, L.C., Read, R.J., (2007). Phaser crystallographic software. *J. Appl. Crystallogr.*, **40**, 658–674.
69. Murshudov, G.N., Skubak, P., Lebedev, A.A., Pannu, N.S., Steiner, R.A., Nicholls, R.A., et al., (2011). REFMAC5 for the refinement of macromolecular crystal structures. *Acta Crystallogr. D Biol. Crystallogr.*, **67**, 355–367.
70. Williams, C.J., Headd, J.J., Moriarty, N.W., Prisant, M.G., Videau, L.L., Deis, L.N., et al., (2018). MolProbity: More and better reference data for improved all-atom structure validation. *Protein Sci.*, **27**, 293–315.
71. Krissinel, E., Henrick, K., (2007). Inference of macromolecular assemblies from crystalline state. *J. Mol. Biol.*, **372**, 774–797.
[72]. Baker, N.A., Sept, D., Joseph, S., Holst, M.J., McCammon, J.A., (2001). Electrostatics of nanosystems: Application to microtubules and the ribosome. *Proc. Natl. Acad. Sci. USA*, **98**, 10037–10041.
73. Winn, M.D., Ballard, C.C., Cowtan, K.D., Dodson, E.J., Emsley, P., Evans, P.R., et al., (2011). Overview of the CCP4 suite and current developments. *Acta Crystallogr. D Biol. Crystallogr.*, **67**, 235–242.
[74]. Jarasch, A., Skerra, A., (2017). Aligning, analyzing, and visualizing sequences for antibody engineering: Automated recognition of immunoglobulin variable region features. *Proteins*, **85**, 65–71.